Journal of Scientific Computing, Vol. 27, Nos. 1–3, June 2006 (© 2006)
DOI: 10.1007/s10915-005-9060-x

Finite-Volume-Particle Methods for Models of Transport of Pollutant in Shallow Water

Alina Chertock,[1] Alexander Kurganov,[2] and Guergana Petrova[3]

Received September 22, 2004; accepted (in revised form) September 27, 2004; Published online January 10, 2006

We present a new hybrid numerical method for computing the transport of a passive pollutant by a flow. The flow is modeled by the Saint-Venant system of shallow water equations and the pollutant propagation is described by a transport equation. The idea behind the new finite-volume-particle (FVP) method is to use different schemes for the flow and the pollution computations: the shallow water equations are numerically integrated using a finite-volume scheme, while the transport equation is solved by a particle method. This way the specific advantages of each scheme are utilized at the right place. This results in a significantly enhanced resolution of the computed solution.

KEY WORDS: Saint-Venant system of shallow water equations; transport of pollutant; finite-volume schemes; particle methods; central-upwind schemes; balance laws.

1. INTRODUCTION

Prediction of a pollution transport in flows is an important problem in many industrial and environmental projects. Different mathematical models are used to describe the propagation of the pollutant and to obtain its accurate location and concentration.

In this paper, we consider the transport of a passive pollutant by a flow modeled by the one-dimensional (1D) Saint-Venant system

[1] Department of Mathematics, North Carolina State University, Raleigh, NC 27695, USA. E-mail: chertock@math.ncsu.edu
[2] Department of Mathematics, Tulane University, New Orleans, LA 70118, USA. E-mail: kurganov@math.tulane.edu
[3] Department of Mathematics, Texas A & M University, College Station, TX 77843, USA. E-mail: gpetrova@math.tamu.edu

$$\begin{cases} h_t + (hu)_x = S, \\ (hu)_t + \left(hu^2 + \dfrac{gh^2}{2} \right)_x = -ghB_x. \end{cases} \tag{1.1}$$

Here h and u are the depth and the velocity of the water, respectively, g is the gravity constant, and S is a source term. The function $B(x)$ represents the bottom topography. The system (1.1) is a simple model, introduced in [15], and is commonly used to describe flows in rivers and coastal areas. For a detailed description of a more realistic shallow water model, derived from the Navier–Stokes equations, we refer the reader to [6].

The propagation of the pollutant is modeled by the transport equation,

$$(hT)_t + (uhT)_x = T_S S, \tag{1.2}$$

which describes the motion of the pollutant concentration T, where T_S is a given concentration of the pollutant at the source. Equations (1.2) and (1.1) are coupled through the source terms.

Designing an *accurate, efficient* and *reliable* numerical method for this model is a challenging task. Solutions of the system (1.1)–(1.2) are typically nonsmooth: they may contain both nonlinear shock and rarefaction waves, and linear discontinuities in the pollution concentration. Moreover, the interaction with a nonflat bottom may result in very complicated wave structures and nontrivial equilibria, which are hard to preserve numerically. In addition, dry states (arising, for example, in dam break problems) need special attention, since (even small) numerical oscillations may lead to nonphysical negative values of the water depth there.

In order to overcome these difficulties, a high-resolution shock-capturing numerical method is required. Such methods for hyperbolic systems of balance laws, and in particular for (1.1), are readily available (to cite a few of them, see e.g. [2, 5, 8, 12, 14]). One of the simplest and the most efficient approaches is to use the *central-upwind schemes* [8, 9]. They can be relatively easily extended to solve (1.1)–(1.2), but the resolution of the computed contact waves in the pollution concentration is not sufficiently sharp. There are some other alternatives (see e.g. [1]), but we are not aware of any method which completely resolves this issue.

Here, we propose such a method. It is a hybrid *finite-volume-particle* (FVP) method, whose core idea is to use central-upwind schemes to solve the system of balance laws (1.1) and a particle method [13] to solve the transport Eq. (1.2). The new method takes an advantage of the nondissipativeness of the particle method, and thus guarantees almost perfect resolution of the contact waves. In [3], the FVP method has been generalized for the two-dimensional (2D) extension of the system (1.1)–(1.2).

The paper is organized as follows. In Secs. 2.1 and 2.2, we give a brief overview of central-upwind schemes and particle methods. Our new method is described in Sec. 2.3, and the numerical computations are carried out in Sec. 3.

2. HYBRID FINITE-VOLUME-PARTICLE METHOD

2.1. Central-Upwind Schemes—An Overview

In this section, we briefly describe the central-upwind schemes for 1D hyperbolic systems of conservation and balance laws. For a complete description of the schemes and their derivation, we refer the reader to [9].

We first consider a 1D system of conservation laws, $u_t + f(u)_x = 0$, which can be rewritten in the equivalent integral form:

$$\bar{u}(x,t+\Delta t)=\bar{u}(x,t)-\frac{1}{\Delta x}\left[\int_{\tau=t}^{t+\Delta t}\left\{f\left(u(x+\tfrac{\Delta x}{2},\tau)\right)-f\left(u(x-\tfrac{\Delta x}{2},\tau)\right)\right\}d\tau\right], \tag{2.1}$$

where $\bar{u}(x,t):=\frac{1}{\Delta x}\int_{I(x)}u(\xi,t)\,d\xi$, and $I(x):=\left\{\xi:|\xi-x|<\Delta x/2\right\}$.

For simplicity, we consider a uniform grid, $t^n:=n\Delta t, x_j=j\Delta x$. If at time level t^n the cell averages, $\bar{u}_j^n:=\bar{u}(x_j,t^n)$, are available, we use them to reconstruct a nonoscillatory piecewise polynomial,

$$\widetilde{u}(x,t^n)=p_j^n(x),\quad x_{j-\frac{1}{2}}<x<x_{j+\frac{1}{2}},\ \ \forall j, \tag{2.2}$$

and evolve it according to (2.1). The nonoscillatory behavior of the central-upwind schemes depends on an appropriate choice of a piecewise polynomial reconstruction—various such reconstructions are available. Note that $\widetilde{u}(\cdot,t^n)$ is, in general, discontinuous at the interface points $\{x_{j+\frac{1}{2}}\}$. The discontinuities propagate with *right-* and *left-sided local speeds*, which, for example, can be estimated by

$$\begin{aligned}a^+_{j+\frac{1}{2}}&=\max\left\{\lambda_N\Big(\frac{\partial f}{\partial u}(u^-_{j+\frac{1}{2}})\Big),\lambda_N\Big(\frac{\partial f}{\partial u}(u^+_{j+\frac{1}{2}})\Big),0\right\},\\ a^-_{j+\frac{1}{2}}&=\min\left\{\lambda_1\Big(\frac{\partial f}{\partial u}(u^-_{j+\frac{1}{2}})\Big),\lambda_1\Big(\frac{\partial f}{\partial u}(u^+_{j+\frac{1}{2}})\Big),0\right\}.\end{aligned} \tag{2.3}$$

Here $\lambda_1<\cdots<\lambda_N$ are the N eigenvalues of the Jacobian $\frac{\partial f}{\partial u}$, and $u^+_{j+\frac{1}{2}}:=p^n_{j+1}(x_{j+\frac{1}{2}})$ and $u^-_{j+\frac{1}{2}}:=p^n_j(x_{j+\frac{1}{2}})$ are the corresponding right and left values of the reconstruction. New cell averages are obtained from (2.1) by integrating over nonuniform rectangular domains, which after an

intermediate reconstruction are projected back onto the original grid. This results in a *fully-discrete* central-upwind scheme, which can be found in [9]. Passing to the limit as $\Delta t \to 0$, we obtain the *semi-discrete* central-upwind scheme:

$$\frac{d}{dt}\bar{u}_j(t) = -\frac{H_{j+\frac{1}{2}}(t) - H_{j-\frac{1}{2}}(t)}{\Delta x},$$

where the numerical fluxes $H_{j+\frac{1}{2}}$ are given by

$$H_{j+\frac{1}{2}}(t) := \frac{a^+_{j+\frac{1}{2}} f(u^-_{j+\frac{1}{2}}) - a^-_{j+\frac{1}{2}} f(u^+_{j+\frac{1}{2}})}{a^+_{j+\frac{1}{2}} - a^-_{j+\frac{1}{2}}} + \frac{a^+_{j+\frac{1}{2}} a^-_{j+\frac{1}{2}}}{a^+_{j+\frac{1}{2}} - a^-_{j+\frac{1}{2}}}\left[u^+_{j+\frac{1}{2}} - u^-_{j+\frac{1}{2}}\right]. \tag{2.4}$$

In [8], the scheme (2.1)–(2.4) has been generalized for the 1D system of balance laws, $u_t + f(u)_x = R(u(x,t), x, t)$. The generalization is

$$\frac{d}{dt}\bar{u}_j(t) = -\frac{H_{j+\frac{1}{2}}(t) - H_{j-\frac{1}{2}}(t)}{\Delta x} + \bar{R}_j(t), \tag{2.5}$$

where $\bar{R}_j(t)$ is an appropriate quadrature for $\frac{1}{\Delta x}\int_{x_{j-\frac{1}{2}}}^{x_{j+\frac{1}{2}}} R(u(x,t), x, t)\,dx$, and the numerical fluxes, $H_{j+\frac{1}{2}}$, are still given by (2.4). However, it should be pointed out that the local speeds, $a^{\pm}_{j+\frac{1}{2}}$, which correspond to the largest and the smallest speeds of the nonlinear waves that appear in the solution of the local generalized Riemann problem, centered at $x = x_{j+\frac{1}{2}}$, can be affected by the presence of the source term, and thus formula (2.3) may require an adjustment.

Remarks.

1. The semi-discretization (2.4)–(2.5) is a system of time dependent ODEs, which should be solved by a sufficiently accurate and stable ODE solver.
2. The (formal) order of the resulting method is determined by the order of the piecewise polynomial reconstruction (2.2) and by the order of the ODE solver.

2.2. Particle Methods—An Overview

Here, we briefly describe the second main ingredient of our new method—the particle method. We consider the initial value problem for the linear transport equation with variable coefficients:

$$\varphi_t + (\xi\varphi)_x = f, \quad \varphi(x,0) = \varphi_0(x). \tag{2.6}$$

First, the initial condition is approximated by a sum of Dirac distributions,

$$\varphi_0(x) \approx \varphi_N(x,0) = \sum_{i=1}^{N} w_i(0)\delta(x - x_i^p(0)), \tag{2.7}$$

with $x_i^p(0)$ being the initial location and $w_i(0)$ being the initial weight of the ith particle ($w_i(0)$ is an integral of $\varphi_0(x)$ over a neighborhood of the point $x_i^p(0)$). Then, an approximate solution φ_N to (2.6) is sought in the form

$$\varphi_N(x,t) = \sum_{i=1}^{N} w_i(t)\delta(x - x_i^p(t)), \tag{2.8}$$

where the evolution of the weights w_i and the locations x_i^p is described by the system of ODEs:

$$\frac{dx_i^p(t)}{dt} = \xi(x_i^p, t), \quad \frac{dw_i(t)}{dt} = \beta_i(t), \tag{2.9}$$

with initial values $(x_i^p(0), w_i(0))$. Here, β_i reflects the contribution of the source term f (see e.g. [13]). In general, (2.9) is to be solved numerically, and at final time t_{fin}, the solution $\varphi(x, t_{\text{fin}})$ is recovered from the computed approximation $\varphi_N(x, t_{\text{fin}})$ (the details are discussed in Sec. 2.3).

2.3. A New Finite-Volume-Particle Method

The new numerical method for (1.1)–(1.2) is a hybrid of the methods in Secs. 2.1 and 2.2: we apply the semi-discrete central-upwind scheme to (1.1), while (1.2) is solved by the particle method. We now present a detailed description of the method.

Following [8, 14], we first rewrite the Saint-Venant system (1.1) in terms of the water surface, $w := h + B$,

$$\begin{cases} w_t + (hu)_x = S, \\ (hu)_t + \left[\frac{(hu)^2}{w-B} + \frac{g}{2}(w-B)^2\right]_x = -g(w-B)B_x. \end{cases} \tag{2.10}$$

The central-upwind scheme (2.4)–(2.5) is then applied to this system. To this end, the quadratures $\bar{R}_j := \left(\bar{R}_j^{(1)}, \bar{R}_j^{(2)}\right)^T$ that appear on the right-hand side of (2.5) should be specified. The quadrature in $\bar{R}_j^{(1)}$ depends on

the type of the source S. An example of a spatially localized source is considered in Sec. 3, Example 2. To compute $\bar{R}_j^{(2)}$, one should use the special quadrature,

$$\bar{R}_j^{(2)} = -g\frac{B(x_{j+\frac{1}{2}}) - B(x_{j-\frac{1}{2}})}{\Delta x} \cdot \frac{\left(w^-_{j+\frac{1}{2}} - B(x_{j+\frac{1}{2}})\right) + \left(w^+_{j-\frac{1}{2}} - B(x_{j-\frac{1}{2}})\right)}{2},$$

where, as before, $w^{\pm}_{j+\frac{1}{2}}$ denotes the right/left value of the piecewise polynomial reconstruction of w at $x_{j+\frac{1}{2}}$. Using the above quadrature guarantees the preservation of the stationary steady-state solution ($w \equiv \text{Const}, u \equiv 0, S \equiv 0$), which corresponds to the "lake at rest" state. This property is especially important when quasi-stationary solutions are concerned (see [8] for details).

Next, we consider the transport equation (1.2) and solve it using the aforementioned particle method with $\varphi := hT$, $\xi := u$, and $f := T_S S$. Note that the method, described in Sec. 2.2 for linear transport equations, can be applied directly to (1.2), since it is, in fact, decoupled from system (2.10). To do that, we need to know the values of the velocity $u(x_i^p(t), t)$ and the functions β_i in (2.9). The velocity u can be calculated from the piecewise polynomial approximation of $w = h + B$ and hu, obtained when solving (2.10). The functions β_i depend on the type of the source term in (1.2). A particular example is considered in Sec. 3, Example 2.

Remark. We use two different grids in our hybrid method. The grid for the central-upwind scheme, $\{x_j\}$, is fixed, while the particle locations, $\{x_i^p(t)\}$, change in time according to the flow.

Recall that after applying the particle method to equation (1.2), only the locations $\{x_i^p(t_{\text{fin}})\}$ of the particles and their weights $\{w_i(t_{\text{fin}})\}$ will be available. Then, the solution $hT(\cdot, t_{\text{fin}})$ at the final time should be recovered by regularizing the particle solution. Such a regularization is performed by a convolution with a "cut-off function", which is taken as a smooth approximation of the δ-function, see [13]. Usually, this procedure works perfectly to recover smooth solutions. However, here we mostly deal with discontinuous solutions, whose discontinuities will be overly smeared by the use of smooth cut-off functions, especially in practice, when a relatively small number of particles is used.

To recover nonsmooth solutions, we implement a different technique. We interpret the weights of the particles, $w_i(t_{\text{fin}})$, as an integral of the solution $hT(\cdot, t_{\text{fin}})$ over the interval $I_i := \left[\frac{x_{i-1}^p(t_{\text{fin}}) + x_i^p(t_{\text{fin}})}{2}, \frac{x_i^p(t_{\text{fin}}) + x_{i+1}^p(t_{\text{fin}})}{2}\right]$,

and thus the cell averages $\overline{hT}_i$ over I_i are

$$\overline{hT}_i = \frac{w_i(t_{\text{fin}})}{|I_i|} = \frac{2w_i(t_{\text{fin}})}{x^p_{i+1}(t_{\text{fin}}) - x^p_{i-1}(t_{\text{fin}})}. \tag{2.11}$$

This will not smear the discontinuities, but may lead to an oscillatory approximation of the solution. When such oscillations appear, we apply the nonlinear filter, proposed in [4], to $\{\overline{hT}_i\}$. To this end, we first reconstruct a piecewise linear interpolant from the cell-averages (2.11), and use it for computing the point values of hT at the original uniform grid points $\{x_{j+\frac{1}{2}}\}$. We then utilize a filter algorithm similar to Algorithm 2.3 in [4]. Notice, that the nonlinear filter is applied only once, as a post-processing, not after every time step as in [4], and only if oscillations are observed. For instance, in Examples 1 and 2 in Sec. 3, we do not apply the filter since the solutions, recovered by formula (2.11), are nonoscillatory.

3. NUMERICAL EXAMPLES

In this section, we illustrate the performance of the new FVP method by a number of numerical examples. We also compare these results with the corresponding solutions computed by the central-upwind scheme, applied to both (2.10) and (1.2). This is a finite-volume method, which will be referred to as FV method.

In our examples, we use the second-order central-upwind scheme that employs the generalized minmod piecewise linear reconstruction [10, 11, 16] and the third-order strong stability-preserving (SSP) Runge–Kutta method for the time evolution (see [7] and the references therein).

We briefly recall that if one has a set of cell averages, $\{\bar{\psi}_j\}$, then the generalized minmod reconstruction is given by $L^n_j(x) = \bar{\psi}_j + s_j(x - x_j)$, with the slopes

$$s_j = \text{minmod}\left(\theta\frac{\bar{\psi}_j - \bar{\psi}_{j-1}}{\Delta x}, \frac{\bar{\psi}_{j+1} - \bar{\psi}_{j-1}}{2\Delta x}, \theta\frac{\bar{\psi}_{j+1} - \bar{\psi}_j}{\Delta x}\right).$$

Here, $\theta \in [1, 2]$, and the multivariate minmod function is defined by

$$\text{minmod}(x_1, x_2, \ldots) := \begin{cases} \min_j\{x_j\}, & \text{if } x_j > 0 \ \forall j, \\ \max_j\{x_j\}, & \text{if } x_j < 0 \ \forall j, \\ 0, & \text{otherwise.} \end{cases}$$

Notice that larger θ's correspond to less dissipative but, in general, more oscillatory limiters. In the presented examples, we took $\theta = 2$.

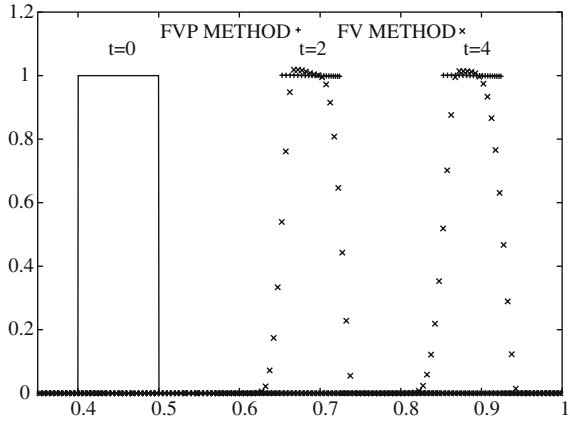

Fig. 1. Pollutant concentration computed by the FVP and FV methods.

Example 1.—Advection of Pollutant. In this example, we assume that the initial water level is constant, $w(x,0)\equiv 1$, the initial discharge is $h(x,0)u(x,0)=0.1$, the gravitational constant $g=1$, the pollution source has been already turned off, $S\equiv 0$, the bottom topography is given by

$$B(x)=\begin{cases}0.25(\cos(10\pi(x-0.5))+1), & \text{if } 0.4\leqslant x\leqslant 0.6,\\ 0, & \text{otherwise,}\end{cases}$$

and the only initially polluted area is $[0.4, 0.5]$, where $T(x,0)=1$.

In time, the initial pollution moves to the right, and we numerically track its propagation. The pollutant concentration at times $t=0, 2$ and 4, computed by the FVP method with 20 "polluted" particles and the FV method, is shown in Fig. 1 (in both methods we take $\Delta x=0.005$ for the central-upwind scheme). One can clearly see the superiority of the results obtained by the FVP method.

Example 2.—Emission of Pollutant. This example is taken from [1]. Here, $w(x,0)\equiv 2$, $h(x,0)u(x,0)=0.5$, $g=1$, and

$$B(x)=\begin{cases}0.2-0.05(x-10)^2, & \text{if } 8\leqslant x\leqslant 12,\\ 0, & \text{otherwise.}\end{cases}$$

We assume that the water is initially clean, but at time $t=100$ a source of polluted water $S=0.01$ with a concentration of pollutant $T_S=10$ is turned on at the point $x=45$. Later on, at time $t=300$, the pollution

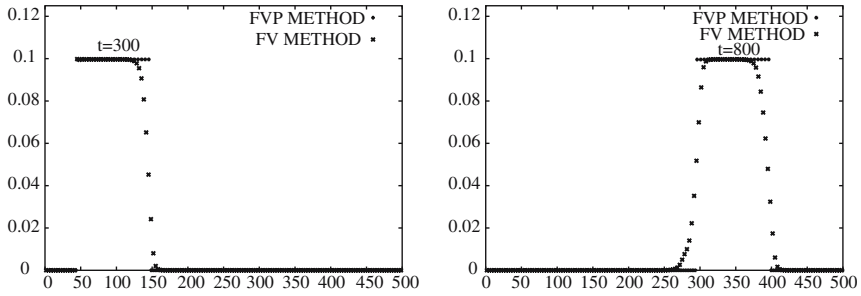

Fig. 2. Pollutant concentration computed by the FVP and FV methods.

source is turned off. The source is, in fact, given by $S(x,t) = 0.01 \cdot \delta(x - 45)$ for $100 \leqslant t \leqslant 300$, and therefore its discretization, required by the central-upwind scheme (2.4)–(2.5), is straightforward. Let the point $x = 45$ be located inside the j_0th cell. Then we have $\bar{R}^{(1)}_{j_0} = 0.01/\Delta x$ and $\bar{R}^{(1)}_{j} = 0$ for all $j \neq j_0$.

As for the particle method for (1.2), the presence of the source will result in the dynamical generation of particles at $x = 45$ according to the following algorithm. A total number of particles N is prescribed in advance, they appear every $\Delta\tau := (\min\{t_{\text{fin}}, 300\} - 100)/(N-1)$, starting at $t = 100$, and their weights are $w_i = 0.1\Delta\tau$. Since the source is localized at one point, the weights of the particles in (2.8) will not change after they are flown away from the source.

In Fig. 2, we present the pollutant concentration computed by the FVP method with 20 "polluted" particles and the FV method at times $t = 300$ and $t = 800$. In both methods, $\Delta x = 10/3$ for the central-upwind scheme. Again, one can clearly see that the FVP method outperforms the FV method by far.

Example 3.—Dam Break. This is an example (also taken from [1]) of a dam break on a flat bottom, where the pollutant has different concentrations on each side of the dam. The initial data correspond to the Riemann problem with $(h, u, T) = (1.0, 0, 0.7)$ if $x < 0$ and $(h, u, T) = (0.5, 0, 0.5)$ if $x > 0$, the gravitational constant $g = 9.8$, and $S \equiv 0$.

We apply the FVP method with initially uniformly distributed "polluted" particles, and the FV method. We use $\Delta x = 10$ for both the central-upwind scheme and the initial distribution of the particles. We first show (Fig. 3) an oscillatory approximation of hT and T at time $t = 240$, computed by the "unfiltered" FVP method. The oscillations, caused by the recovering procedure (2.11), can be successfully removed by the nonlinear

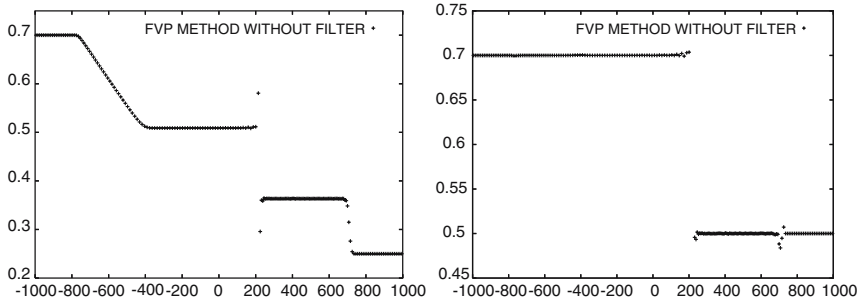

Fig. 3. hT and T at $t = 240$ computed by the "unfiltered" FVP method.

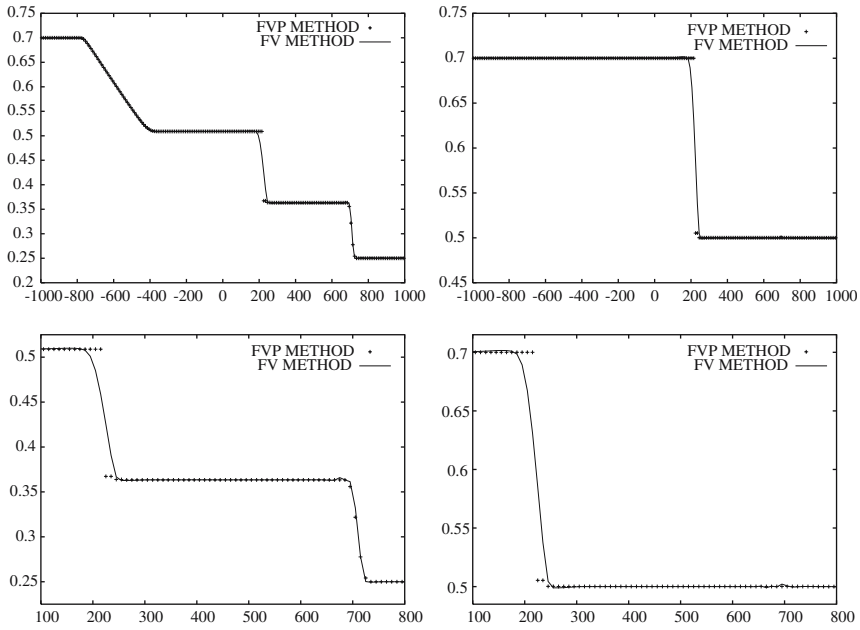

Fig. 4. hT and T at $t = 240$ computed by the FVP and FV methods (a, b). Zoom at the discontinuous areas (c, d).

filter, as shown in Fig. 4, where we also compare the solutions, obtained by the FVP and the FV methods. Once again, the advantage of the FVP method can be clearly seen.

ACKNOWLEDGMENTS

The work of A. Chertock was supported in part by the NSF Grant # DMS-0410023. The research of A. Kurganov was supported in part by the NSF Grants # DMS-0196439 and DMS-0310585. The work of G. Petrova was supported in part by the NSF Grant # DMS-0296020.

REFERENCES

1. Audusse, E., and Bristeau, M. (2003). Transport of pollutant in shallow water. A two time steps kinetic method. *M2AN Math. Model. Numer. Anal.* **37**, 389–416.
2. Bale, D. S., LeVeque, R. J., Mitran, S., and Rossmanith, J. A. (2002). A wave propagation method for conservation laws and balance laws with spatially varying flux functions. *SIAM J. Sci. Comput.* **24**, 955–978.
3. Chertock, A., and Kurganov, A. (2004). On a hybrid finite-volume-particle method. *M2AN Math. Model. Numer. Anal.* **38**, 1071–1091.
4. Engquist, B., Lötstedt, P., and Sjögreen, B. (1989). Nonlinear filters for efficient shock computation. *Math. Comp.* **52**, 509–537.
5. Gallouët, T., Hérard, J.-M., and Seguin, N. (2003). Some approximate Godunov schemes to compute shallow-water equations with topography. *Comput. Fluids*. **32**, 479–513.
6. Gerbeau, J. F., and Perthame, B. (2001). Derivation of viscous Saint-Venant system for laminar shallow water; numerical validation. *Discrete Contin. Dyn. Syst. Ser. B* **1**, 89–102.
7. Gottlieb, S., Shu, C.-W., and Tadmor, E. (2001). High order time discretization methods with the strong stability property. *SIAM Rev.* **43**, 89–112.
8. Kurganov, A., and Levy, D. (2002). Central-upwind schemes for the Saint-Venant system. *M2AN Math. Model. Numer. Anal.* **36**, 397–425.
9. Kurganov, A., Noelle, S., and Petrova, G. (2001). Semi-discrete central-upwind scheme for hyperbolic conservation laws and Hamilton-Jacobi equations. *SIAM J. Sci. Comput.* **23**, 707–740.
10. van Leer, B. (1979). Towards the ultimate conservative difference scheme, V. A second order sequel to Godunov's method. *J. Comput. Phys.* **32**, 101–136.
11. Nessyahu, H., and Tadmor, E. (1990). Non-oscillatory central differencing for hyperbolic conservation laws. *J. Comput. Phys.* **87**, 408–463.
12. Perthame, B., and Simeoni, C. (2001). A kinetic scheme for the Saint-Venant system with a source term. *Calcolo*. **38**, 201–231.
13. Raviart, P. A. (1983). An analysis of particle methods. In Brezzi, F. (ed.), *Numerical Methods in Fluid Dynamics*, Lecture Notes in Mathematics, Vol. 1127, Springer-Verlag GmbH, Heidelberg, pp. 243–324.
14. Russo, G. (2001). Central schemes for balance laws. *Hyperbolic problems: Theory, numerics, application*, Vol. II (Magdeburg, 2000), Internat. Ser. Numer. Math. 141, Birkhauser, Basel, pp. 821–829.
15. de Saint-Venant, A. J. C. (1871). Théorie du mouvement non-permanent des eaux, avec application aux crues des rivière at à l'introduction des marées dans leur lit. *C.R. Acad. Sci. Paris.* **73**, 147–154.
16. Sweby, P. K. (1984). High resolution schemes using flux limiters for hyperbolic conservation laws. *SIAM J. Numer. Anal.* **21**, 995–1011.